Ultrawideband Array With 70° Scanning Using FSS Superstrate

Ersin Yetisir, *Member, IEEE*, Nima Ghalichechian, *Senior Member, IEEE*, and John L. Volakis, *Fellow, IEEE*

***Abstract*— We present a wideband tightly coupled dipole array (TCDA) with integrated balun and a novel superstrate consisting of printed frequency selective surface (FSS) for wide angle scanning. Although previous TCDAs have had decent scanning performance up to ±60°, use of dielectric superstrates are usually required, resulting in additional cost and fabrication complexity. In this paper, we replace the bulky dielectric layer(s) with periodic printed elements and yet achieve wide-angle and wideband impedance matching. The proposed approach provides superior performance of 6.1:1 bandwidth (0.5–3.1 GHz) with VSWR < 3.2 when scanning ±75° in *E* plane, ±70° in *D* plane and ±60° in *H* plane. The FSS, radiating dipoles and feed lines are designed and fabricated on the same vertically oriented printed circuit board, resulting in a low-cost and lightweight structure as compared to other low profile arrays. Measured scanning patterns of a 12 × 12 prototype are presented, showing good agreement with simulations.**

***Index Terms*— Low profile arrays, ultrawideband antennas, wide angle scanning arrays.**

I. Introduction

FUTURE mobile and stationary communication platforms are expected to have multiple sensors to cover the desired frequency bands and/or scanning range. To address this, novel approaches like the advanced multifunction RF concept were proposed to reduce the number of antenna apertures and RF/digital hardware for communication, radar, and electronic warfare [1]. Ideally, this concept requires a wideband phased array to provide single aperture for multiple operating frequencies and communication links in different directions. In other words, a very wideband antenna array with large scan volume is an essential component of such systems.

A tapered slot array, also known as Vivaldi, is a popular wideband scanning antenna. Different versions of this array focus on bandwidth, modularity, scanning, or power handling [2]–[4]. These arrays can typically cover 10:1 impedance bandwidth with ±60° scan angle [3]. However, they suffer from low polarization purity when scanning in the intercardinal plane, even for moderate elevation angles. Although correction algorithms have been proposed for dual-polarized arrays, they do not provide simultaneous coverage across the entire bandwidth and scan volume [5].

Manuscript received September 30, 2015; revised February 14, 2016; accepted July 10, 2016. Date of publication July 27, 2016; date of current version October 4, 2016.

The authors are with the ElectroScience Laboratory, Department of Electrical and Computer Engineering, The Ohio State University, Columbus, OH 43212 USA (e-mail: yetisir.3@osu.edu; ghalichechian.1@osu.edu; volakis@ece.osu.edu).

Color versions of one or more of the figures in this paper are available online at http://ieeexplore.ieee.org.

Digital Object Identifier 10.1109/TAP.2016.2594817

More recently, low profile versions of Vivaldi arrays have been proposed to address the cross-polarization issue. One particular example is the decade bandwidth BAVA array [6], using an impedance matching approach similar to Vivaldi. The total height is less than half a wavelength at the highest frequency of operation, resulting in excellent polarization purity. However, the BAVA array has poor impedance matching when scanning across the *H* plane, limiting their typical scanning range to 45°.

Another class of wideband arrays is referred to as connected arrays. One example of these is the long slot array that exhibits large impedance bandwidth [7]. However, the bandwidth is reduced to less than 50% when the array is backed by a conducting plane. A ferrite loaded substrate can be used to mitigate ground plane effects and provide 10:1 impedance bandwidth with 60° scan angle [8]. However, ferrites are typically heavy and increasingly lossy at higher frequencies.

Munk *et al.* [9] proposed capacitively coupled dipoles instead of electrically connected radiators. The idea was to mitigate reactive (inductive) loading from the ground plane using capacitive coupling among neighboring elements. Since the antenna elements are closely spaced and tightly coupled, the current on the dipoles is almost constant, realizing Wheeler's current sheet [10]. Munk's concept could achieve up to 4.5:1 impedance bandwidth [11]. But adding two dielectric slabs above the array aperture can increase the bandwidth to 9:1 with scan angles up to 60°. However, external wideband 180° hybrids were required to avoid common mode resonances along the feed lines of the dipoles. As a result, the feed is bulky and expensive.

To avoid complex baluns, different approaches have been proposed. One approach is to place shorting pins between the dipole aperture and the ground plane to shift the common mode resonance out of the operational band [12]. This approach provides 5:1 impedance bandwidth and ±45° scanning using a single layer of dielectric superstrate and a single stage matching circuit. The latter is printed after the feed lines and below the ground plane. However, the radiating elements are embedded inside dielectric slabs having a relative dielectric constant of $\varepsilon_r \geq 1.96$. The substrate and superstrate layers of the array combine to form a thick dielectric slab over the ground plane. This leads to surface waves (SWs), even for moderate scan angles [13]. To address this issue, perforations across the dielectric layers were proposed to reduce the effective dielectric constant and push the onset of SWs out of the intended scan range and frequency band. However, practical arrays are still

limited to less than 60° [12], and therefore, not suitable for wider angles. Munk's coupled dipole concept was recently enhanced with an integrated feed [14]. Specifically, a printed circuit board (PCB) implementation of folded Marchand balun [15] was used to excite the dipoles. The balun was in effect a two-stage impedance matching circuit. It was optimized together with other array parameters to achieve an impressive 7.35:1 impedance bandwidth. However, scanning was limited to 45°. Single layer of dielectric superstrate was used to compensate impedance variation while scanning. It is important to note that the radiating elements of each unit cell were split into two small dipoles along the E plane, following the approach proposed in [16]. This was done to reduce the input impedance for easier matching. The dipole pair was then fed by a Wilkinson power divider. However, this approach caused resistive loss while scanning in the E plane. Although the reported resistive loss was <0.5 dB up to 45°, it increases for larger elevation angles. A similar feeding mechanism was used in [17] with resistive frequency selective surface (FSS) inside the substrate of the array. The bandwidth was 13.9:1 but increasing loss was again limiting wide angle scanning. This paper builds on the work of [14] and [17] but provides several new contributions to enable wide-angle scanning for low-loss, wideband arrays. Among them are: 1) an FSS above the tightly coupled dipole array (TCDA) to replace dielectric the superstrate; 2) elimination of the Wilkinson power divider; and 3) a modified stripline-based Marchand balun for wideband impedance matching.

This paper is organized as follows. Section II introduces the basic structure and parameters of the unit cell for the new TCDA. Measured data are then presented in Section III, using a 12 × 12 prototype. Our conclusions are provided in Section IV.

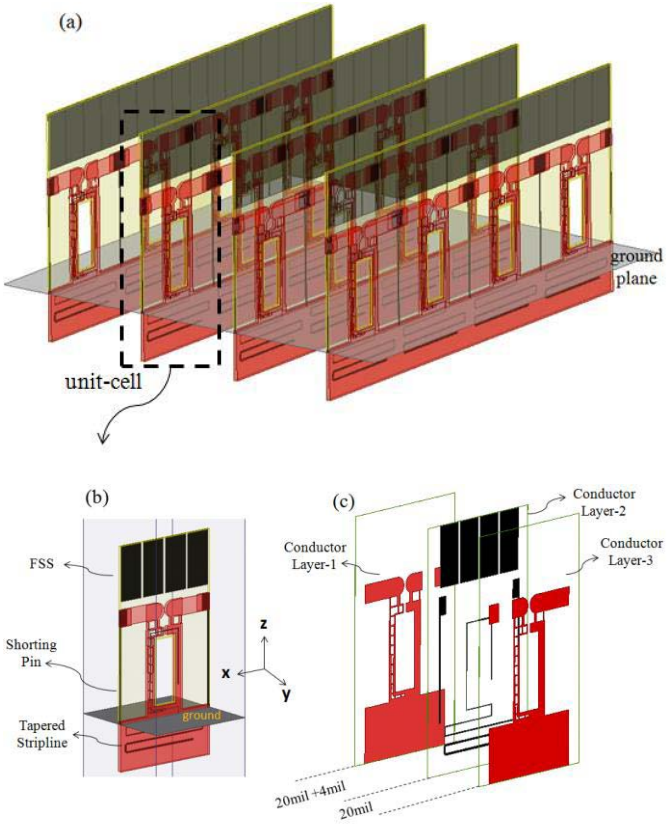

Fig. 1. TCDA with FSS superstrate. (a) 4 × 4 array. (b) Unit cell. (c) Copper layers forming the PCB.

II. FSS Integrated Tightly Coupled Dipole Array

As already noted, this paper proposes a new array that builds on the TCDA concept in [14] and [17]. Of importance is the replacement of the dielectric superstrate by an FSS while still using a single PCB. This approach is of much lower cost and also provides for larger scan volumes. The integrated Marchand balun operates similar to the one described in [14] but has a modified structure so that the Wilkinson power splitter is removed. More important, the FSS, dipoles, and balun are fabricated on the same PCB. The height of the array above the ground plane is $0.67\lambda_{\text{high}}$ with a $0.11\lambda_{\text{high}}$ meandered stripline below the ground. The unit cell is a $0.43\lambda_{\text{high}} \times 0.43\lambda_{\text{high}}$ square, chosen to be smaller than half-wavelength to ease scanning in the E plane.

The proposed TCDA with FSS superstrate is depicted in Fig. 1. It is a single-pol array, implemented using three-layer PCB technology. Three copper layers are hosted by two RT/duroid 5880 (20 mil and $\varepsilon_r = 2.2$) substrates. These layers are bonded using a 4-mil-thick polyflon material, resulting in 44 mil overall thickness for the PCBs. They are vertically placed over the ground plane [see Fig. 1(c)]. We remark that the low ε_r of RT/duroid 5880 makes it possible to design high-impedance striplines within standard fabrication tolerances. However, other materials with reasonably low dielectric constant (e.g., Rogers 4003C and $\varepsilon_r = 3.55$) can be used.

Wideband impedance performance was achieved by codesigning and tuning capacitively coupled dipoles, ground plane height, printed FSS layer, and the Marchand balun. We note that the FSS superstrate was chosen to operate well below its resonance frequency. This is necessary as it is intended to provide shunt capacitance for a plane wave propagating along (or close to) the z-axis. This reduces the characteristic impedance of the medium, in the same manner as a dielectric superstrate does. As already noted, added capacitance mitigates the inductive loading due to the ground plane.

The Marchand balun and the shorting pins were used to push any resonant common modes out of the frequency band of interest (0.5–3.25 GHz) as described in [18]. We further note that the employed balun is in effect a multistage matching network as proposed in [14]. It can be seen that one side of the balun, carrying the incoming stripline, is perforated (see Fig. 2). This modified stripline has higher characteristic impedance as compared to a regular stripline of same dimensions and PCB substrate. As emphasized later, these perforations are critical for matching the dipole to a 50-Ω standard microstrip or coaxial cable feed. Therefore, they serve to eliminate the earlier use of a Wilkinson power divider for impedance matching [14].

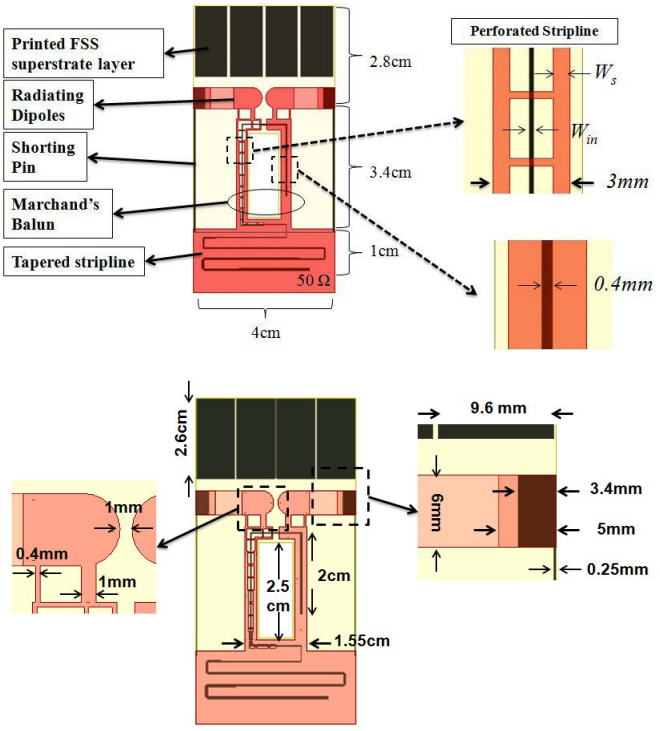

Fig. 2. Detailed geometry of the unit cell for the TCDA with FSS.

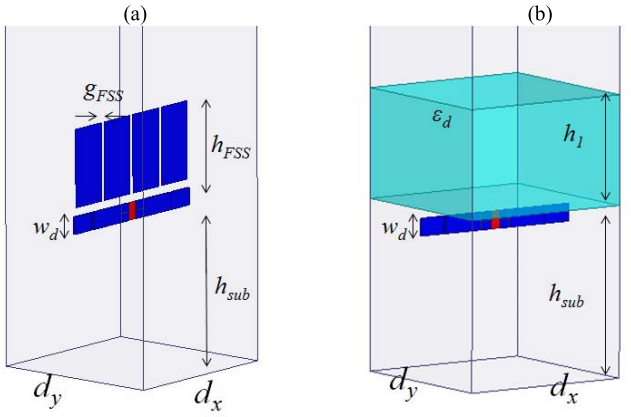

Fig. 3. Unit cell of TCDA with (a) FSS and (b) dielectric superstrate. Feed lines are excluded for simplicity. $d_x = d_y = 0.5\lambda_{\text{high}}$.

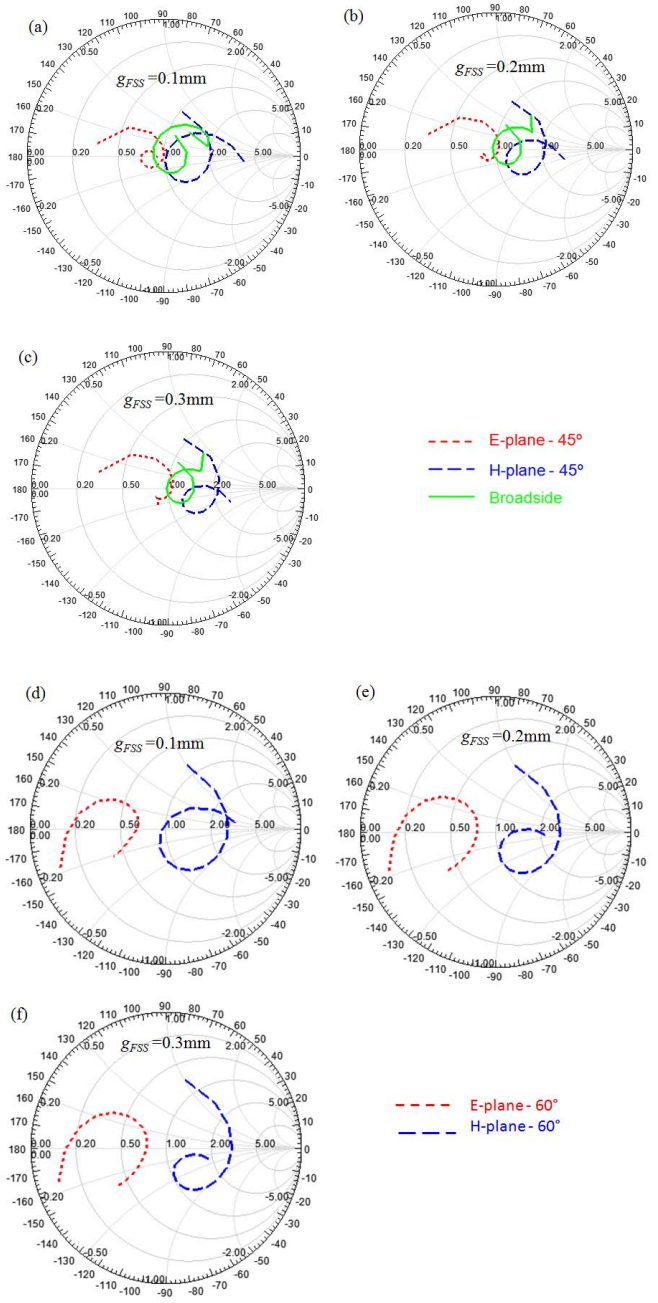

Fig. 4. S_{11} of the TCDA with FSS superstrate across 0.9–3.75 GHz. Data are given for different coupling gaps (g_{FSS}) while h_{FSS} was kept constant at 2 cm. The scan angle was (a)–(c) 45° and (d)–(f) 60°.

A. Printed FSS Layer as Superstrate

It is well known that dielectric layers can improve the total scan volume of a dipole (or slot) array [19]. Stacked parasitic elements above apertures can also be used (particularly for patch antennas) to improve bandwidth and scanning [20], [21]. Recently, a slot array with multiple stratified patch layers as superstrate was proposed [22]. Cavallo *et al.* [22] achieved 2.2:1 impedance bandwidth up to 50° scan angle. The slabs of printed patch layers are simply anisotropic artificial dielectrics [23] incidence. However, the periodicity of these patches along the aperture normal is typically very small (<0.01λ) [24]. This results in a large number of PCB stratifications and increased cost.

Instead of multiple planar layers, we propose to use a single layer of a printed superstrate consisting of vertically oriented conductors [see Fig. 3(a)]. The periodicity of these vertical printed elements is d_y along the H plane and $d_x/4$ along the E plane, where d_x and d_y are unit-cell dimensions of the infinite dipole array. In contrast to [22], the feature size of the periodic elements is rather large. As a result they cannot be approximated as an anisotropic dielectric material. Therefore, we refer to it as FSS throughout this paper, even though it always operates below its resonance frequency and provides capacitive loading.

The proposed FSS was simulated together with the TCDA [Fig. 3(a)]. For simplicity, the feed-lines were excluded as the focus was on studying the FSS. To verify the performance of the FSS, the same TCDA was also simulated using a uniform

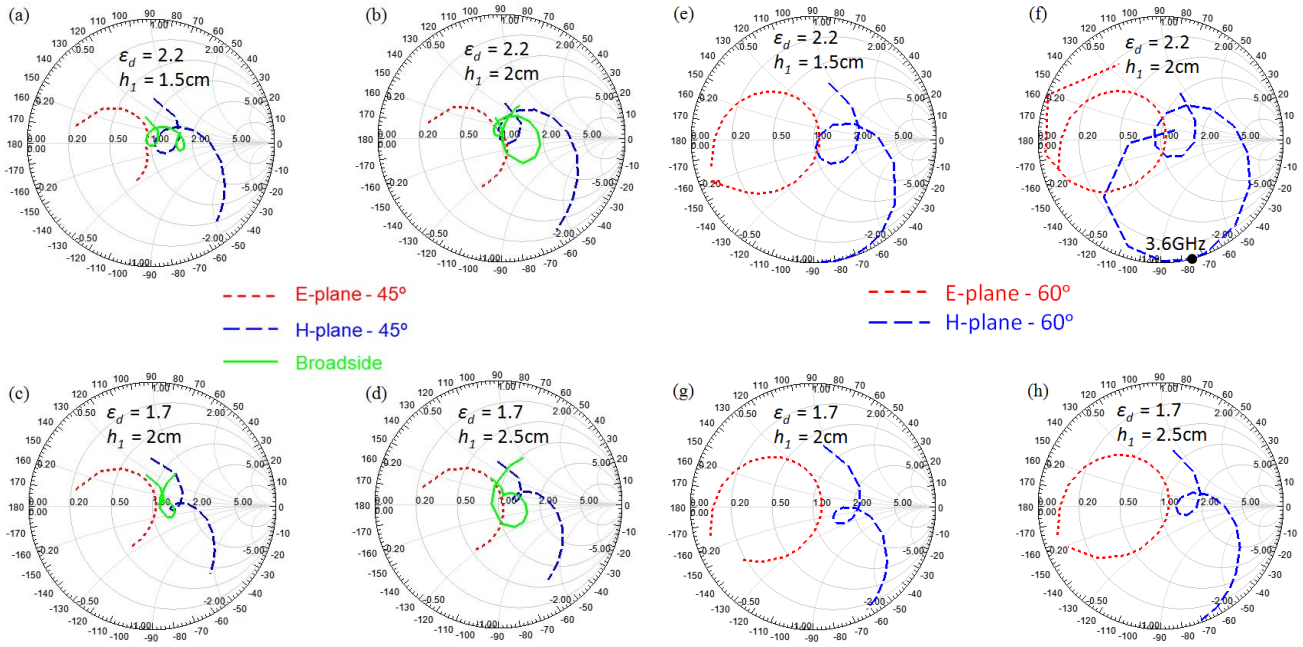

Fig. 5. S_{11} of the TCDA with the dielectric superstrate of different dielectric constants (ε_d = 1.7 and 2.2) and slab thicknesses (h_d = 1.5, 2, and 2.5 cm) across 0.9–3.75 GHz. The scan angle is (a)–(d) 45° and (e)–(h) 60°.

dielectric superstrate [Fig. 3(b)]. We note that if the FSS is to replace the dielectric superstrate, it should provide better (or at least similar) frequency/angular response when placed across an array aperture.

In our parametric full-wave simulations of the TCDAs with FSS and dielectric loading, only the superstrate layers were modified. The ground plane height, balun geometry, and dipole dimensions were all the same and kept constant for both arrays in Fig. 3. The specific values were: 0.9 GHz $< f <$ 3.75 GHz, $d_x = d_y = 4$ cm, and $h_{\text{sub}} = 3.5$ cm. We note that the lattice dimensions (d_x, d_y) are half-wavelength at the highest frequency, typical for a wideband phased array. The variables were ε_d and h_1 for the dielectric slab, and g_{FSS} for the FSS (see Fig. 3).

The simulated data for the input impedance of both arrays is provided in Figs. 4 and 5 up to 60° scanning. A quick glance at the plots reveals that the impedance locus of the FSS array is more confined as compared to the dielectric-loaded array, implying better bandwidth during scanning. A more detailed inspection shows the main difference is at the higher end of the band, especially for larger scan angles. Specifically, as the frequency increases, dielectric-loaded arrays detune due to higher order modes starting to dominate. This detuning is more obvious for higher contrast dielectric ($\varepsilon_r = 2.2$) with the reflection coefficient reaching unity at $f \sim 3.6$ GHz [see Fig. 5(e) and (f)]. This is expected, since it is easier for Floquet modes to couple to an SW mode when the substrate/superstrate material is thicker or has higher dielectric constant [13]. Another important observation is that although Fig. 4(d)–(f) seems more promising than Fig. 5(e)–(h), it is also clear that the FSS-loaded array is not well matched either. In other words, FSS-loaded array has different impedance response during 60° scanning along E and H planes. However, we note that the substrate layer of a fully integrated array typically have vertically oriented feed-lines. These conducting feed-lines also have a different response to TE (H plane scanning) and TM (E plane scanning) Floquet modes [14], which can be used as an additional parameter when designing the array for wide-angle scanning. Therefore, the impedance matching seen at Fig. 4(d)–(f) can be improved once a practical feeding structure is integrated to the unit-cell of the array, as shown in the next sections.

B. Folded Marchand Balun With Perforations

We used a stripline-based Marchand balun to feed the wideband array. Similar approaches were proposed before in [14] and [17] using striplines as transmission lines for the incoming input signal. However, as noted before, [14] and [17] used Wilkinson power dividers to achieve impedance matching to dipoles. To avoid losses due to the power divider during scanning, we pursued an alternative approach. Specifically, we placed rectangular perforations on the ground layer of a stripline (Fig. 2) to increase the achievable characteristic impedance (Z_0). This way, the high dipole impedance can be fed by a single balun without employing dual low-impedance dipoles in each unit cell. Z_0 values for different perforation dimensions are shown in Fig. 6. As seen, the maximum Z_0 can be increased from 110 Ω to more than 160 Ω without changing fabrication tolerances.

A possible drawback of the perforated stripline is the lack of shielding for the inner conductor. This may cause coupling to the substrate region and excitation of a resonant common mode. To examine this, we simulated the TCDA using a perforated balun for multiple scan angles. The resulting

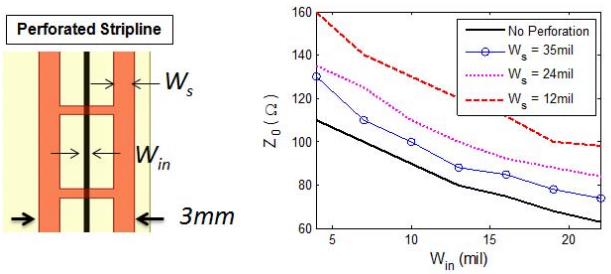

Fig. 6. Characteristic impedance of the perforated stripline for different inner and outer conductor geometry. The parameters are based on Fig. 2 with the PCB substrate is 44 mil thick ($\varepsilon_r = 2.2$).

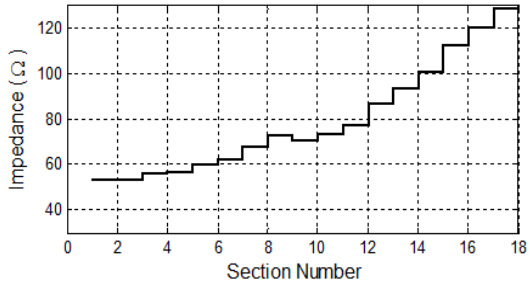

Fig. 8. Impedance profile of the 18-sections stepped transformer. Stripline feed was used to match the TCDA to 50-Ω coaxial cable.

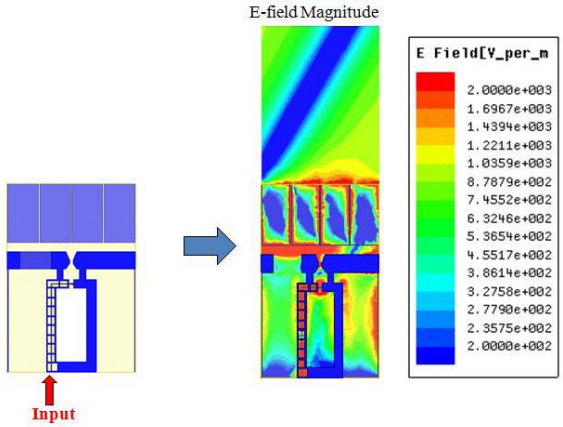

Fig. 7. Field distribution across the array unit cell when scanning to 60° in the E plane at 3 GHz. The incoming electric field via the stripline is well confined within the balun. This indicates that the perforations do not cause significant coupling between the substrate of the array and the inner conductor.

electric field distribution inside the signal line of the balun and the substrate region is depicted in Fig. 7. This plot refers to the case of 60° scan angle in the E plane with 0.4λ unit-cell size. As shown, the electric field of the incoming stripline is well confined inside the balun. This indicates that perforating the balun may not be an issue. However, resonances can still exist if the separation between feed lines of neighboring unit-cells is large enough to support a common mode. To avoid this, we used shorting pins (see Fig. 1) at the boundaries of the neighboring unit cells. This was done in an effort to suppress possible common modes. The shorting pins were placed at the edges of the unit-cells but in the middle layer of the PCBs. Therefore, they are capacitively coupled to the dipole arms that are placed on the outer layers. This helps the dipole performance on the lower end of the bandwidth: When the shorting pins are electrically connected to the dipole arms, they create resonant loops with the balun at low end of the frequency band. However, when placed on the middle layer, they are practically along the virtual ground of the differentially excited dipole arms. Therefore, coupling to the pins is very small, implying minimal effect on the impedance behavior of the dipoles.

C. Infinite Array Design

Having verified the FSS performance and the perforated Marchand balun, we proceeded to optimize the array for maximum bandwidth and scan volume. Specifically, all parameters of the TCDA shown in Fig. 1 were tuned, except for the tapered stripline below the ground plane. Our process involved optimization at three scanning cases: broadside and 60° scan in the E and H planes. The final dimensions are given in Fig. 2.

The input impedance for the tuned array was found to be around 150 Ω. To match this array to 50 Ω, we designed an 18-section stepped transformer as part of the stripline feed. The electrical length of each section was 18° at 1 GHz, making them 1 cm each for the PCB substrate ($\varepsilon_r = 2.2$). This 18-cm-long transformer included the meandered line below the ground and the perforated stripline on one side of the balun (see Fig. 2). The impedance profile of the transformer is plotted in Fig. 8. As shown, the optimized curve resembles an exponential function, indicating that a continuous, exponentially tapered line could also be used. We note that the TCDA array and the transformer were designed separately. Because of this, there is a small decrease in efficiency as compared to the case when the TCDA is excited by a gap source. This is because our meandered feed line is not an ideal transition between 50 and 150 Ω. However, if the array and the transformer were optimized synergistically, the overall efficiency or bandwidth can be further improved.

The simulated mismatch efficiency of the TCDA with the FSS, balun, and transformer is given in Fig. 9. We observe that for scan angles of $\theta \leq 45°$, the bandwidth is 6.5:1 (0.5–3.25 GHz) with VSWR < 3.2 (1.4-dB (1.4-dB mismatch loss). For $\theta \leq 60°$, the bandwidth reduces to 6.4:1 assuming the same level. When scanning beyond 60°, we observe some additional mismatch losses, up to 2.5 dB for the H plane. Concurrently, E and D plane mismatch efficiency is still better than -1 dB for most of the bandwidth.

The normalized cross-polarized gain in the D plane was calculated using Ludwig's third definition [27] and is shown in Fig. 10. As seen, the normalized cross-pol gain is around -14 dB at 45° and -9 dB at 60° scans except at the very high end of the 0.5–3.25-GHz band. These values are close to the ideal linearly polarized dipole apertures where the cross-pol levels are -15 and -10 dB at 45° and 60°, respectively. Degradation of 1 dB is due to the vertically oriented conducting sheets in the FSS layer. However, reduced polarization purity above 2.7 GHz is caused by the feed structure starting to support common modes due to a resonance around 3.5 GHz (out of the intended band). As already noted, this issue can be addressed by small reduction of the distance

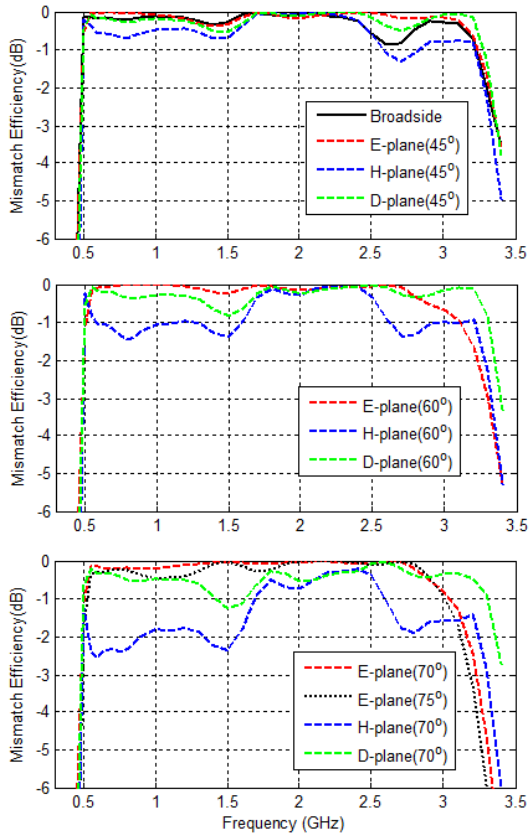

Fig. 9. Mismatch efficiency of the optimized TCDA at various scan angles along the principal and intercardinal planes.

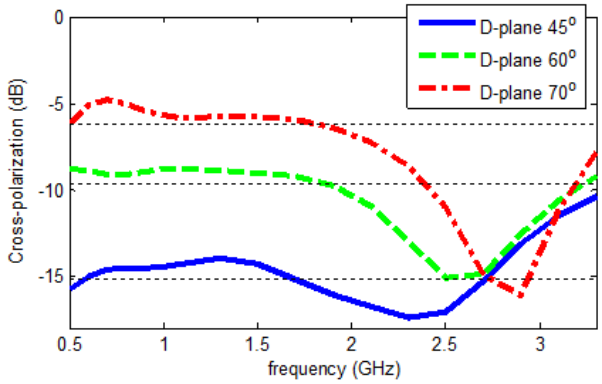

Fig. 10. Normalized cross-polarization ratio along the diagonal plane at 45°, 60°, and 70° scans. Dashed curves show the cross-pol levels of an ideal, linearly polarized aperture scanning along diagonal plane, based on Ludwig's third definition [27].

between the shorting pins and the balun legs and then retuning the unit-cell parameters for the same bandwidth. However, for the scope of this paper, the cross-pol level below −9 dB for scan angle $\theta \leq 60°$ was acceptable and no further attempts for improvement were made.

Although the noted wideband and wide-scan performance of the FSS-loaded array is impressive, it is important to quantify the improvement using a figure of merit value. To do this, we use the metric from [11]

$$P_A = \frac{B|\log(1-\eta_{\min})|}{2\cos\theta_{\max}} \quad (1)$$

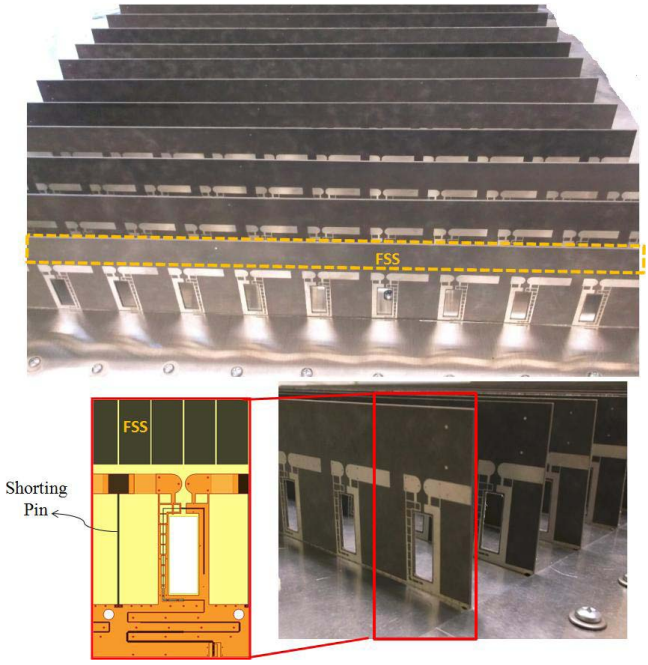

Fig. 11. Fabricated 12 × 12 prototype.

TABLE I
COMPARISON OF STATE-OF-THE-ART WIDE-ANGLE ARRAYS

Design	Loss (dB)	BW	Thickness (λ_{low})	θ_{max}	Figure of Merit (P_A)
This work	1.9	6.4:1 (6.1:1)	0.12	H-60° E-60° (H-60° E-75°)	2.24
[26]	0.5*	1.6:1	0.3	H-60° E-70°	1.09
[3]	1*	7.6:1	0.43	H-60° E-60°	3.85
[25]	2.5	6:1	0.17	H-60° E-60°	1.68
[22]	0.5*	2.2:1	--	H-50° E-50°	1.45

* Only includes mismatch loss since ohmic losses were not available

where $B = (f_{\max} - f_{\min})/\sqrt{f_{\max} f_{\min}}$, $\theta_{\max}$ is the scan angle, and $\eta_{\min}$ is the minimum efficiency for the claimed impedance bandwidth and scan range. This minimum efficiency includes mismatch and ohmic losses. For the proposed work, the overall loss is 1.9 dB at 60° scan angle in the H plane and at the very high end of the frequency band of interest. In the E and D planes, the overall loss is mostly below 1 dB for $\theta_{\max} \leq 60°$.

Table I shows the performance parameters of the proposed array using the figure of merit from (1). The P_A value from previous work on scanning arrays for $\theta_{\max} > 45°$ is also provided. As seen, our FSS-loaded FSS-loaded array outperforms all of the referenced literature, except [3] which refers to an antenna array of However, we note that the impressive performance in [3] refers to a much thicker antenna array.

III. FABRICATED PROTOTYPE AND MEASURED RESULTS

A 12 × 12 prototype was constructed as depicted in Fig. 11. The array includes 12 vertically placed and equally spaced PCBs over the ground plane, each hosting 12 unit cell

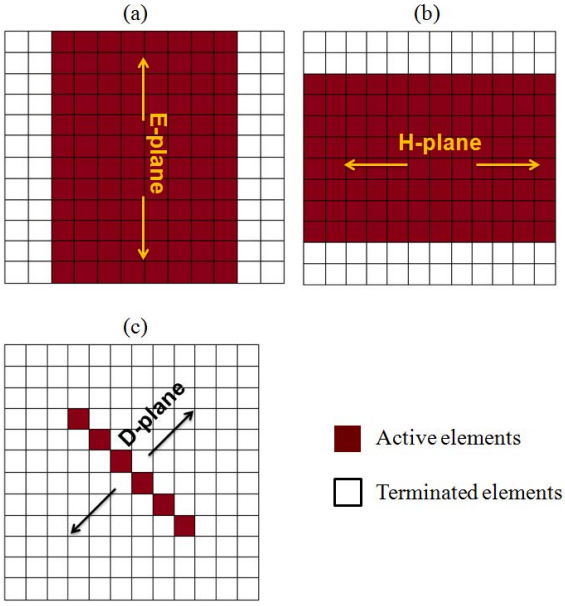

Fig. 12. Active elements of the 12 × 12 prototype during (a) E-, (b) H-, and (c) D-plane measurements are shown with dark color. For D plane, only one row is used to acquire an active element pattern, instead of the scanning pattern of the full array.

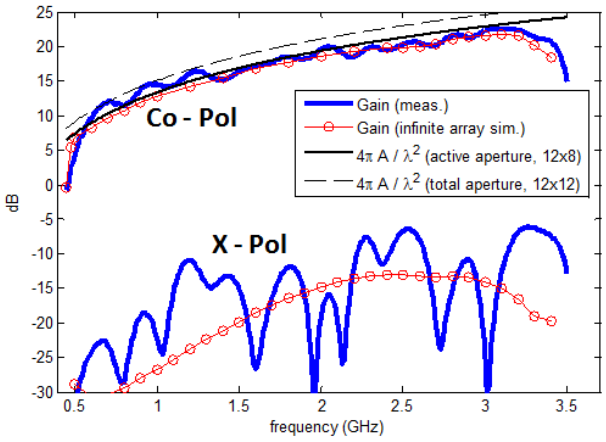

Fig. 13. Broadside gain of the prototype. Measured values agree well with the simulations (generated from infinite array simulations) at high frequencies. At low frequencies, gain approaches the aperture limit of total array (12 × 12).

elements. The aperture was 0.23 m^2 and the ground plane extension was 15 cm on each side from the aperture.

The Ohio State University anechoic chamber was used for pattern measurements. The active part of the aperture was chosen to be 8 × 12 with the longer side of the active array aligning in the scanning plane [see Fig. 12(a) and (b)]. The measured E and H plane scanning patterns of the array were obtained using the unit-excitation unit-excitation active element pattern (UEAEP) method [28]. Typically, UEAEP of each radiating element should be and combined during postprocessing, implying 96 measurements to obtain the radiation pattern of the array for each scanning plane. However, as we are only interested in the E and H plane patterns, certain unit elements have always the same phase/amplitude when scanning in these planes. Therefore, they can be excited by a power divider and measured together. Specifically, when scanning in the E plane, each radiator in an active eight-unit-element row [see Fig. 12(a)] has same phase and amplitude for a uniformly excited array. Therefore, they can be excited by an divider (Mini-Circuits ZN8PD1-53+). Since there are 12 of these eight-element rows, the required number of measurements is 12 instead of 96. The same analysis is also true for the H plane, where the eight-element columns [see Fig. 12(b)] replace the eight-element rows. In this manner, we were able to create scanning plots in the principal planes (E and H) for any elevation angle without a need to measure each unit-cell separately.

For the D plane, only one row along the diagonal of the aperture was excited to obtain the element pattern [see Fig. 12(c)]. Six elements were excited together due to lack of a true center element in the 12 × 12 array. The reason for combining multiple elements is that each off-center element has different beam shapes; slightly tilted main beams from broadside and different X-pol levels depending on their location on the aperture. These differences are less noticeable at higher frequencies, indicating that they are due to the prototype being small in size without edge element termination. When multiple elements are used as a single radiator [see Fig. 12(c)], edge effects on each element are averaged out as they are not strongly correlated. We also note that the six-element linear subarray is aligned orthogonal to the D plane. Therefore, it has the same radiation pattern (only along this plane) with a single element placed at the center of a large array.

The measured gain at broadside is depicted in Fig. 13. As can be seen, the simulated and measured data agree well for most of the bandwidth. At lower frequencies, the measured gain exceeds the active aperture area limit and reaches up to total area (12 × 12) directivity. This was expected, since prototype antenna is electrically small at the lower end of the frequency band. Therefore, even if the edge elements are not excited, they still contribute to the array radiation due to coupling from active elements. The ground plane can also cause unintended radiation, since it extends only a quarter wavelength (at 500 MHz) away from the aperture and has no edge treatment. The predicted normalized cross-polarization (X-pol) isolation was 34 dB, but measured data was only 26 dB. This was due to the feed antenna (ETS Lindgren 3164 Dual Polarized Horn) used during the measurements. The polarization purity of this horn antenna is reported to be 26 dB, limiting the X-pol measurement. Nevertheless, the bottleneck for the performance is the D plane. Our simulated values for the D plane were approximately −10 dB when scanning to 60° elevation angle. This indicates that 26-dB cross-polarization isolation for the feed antenna was sufficient.

Figs. 14 and 15 show the measured and simulated E and H plane patterns at different frequencies. At each frequency, the 2-D patterns are normalized to the broadside gain. Beamwidths and gain levels of the measured and simulated patterns are in very good agreement. As expected,

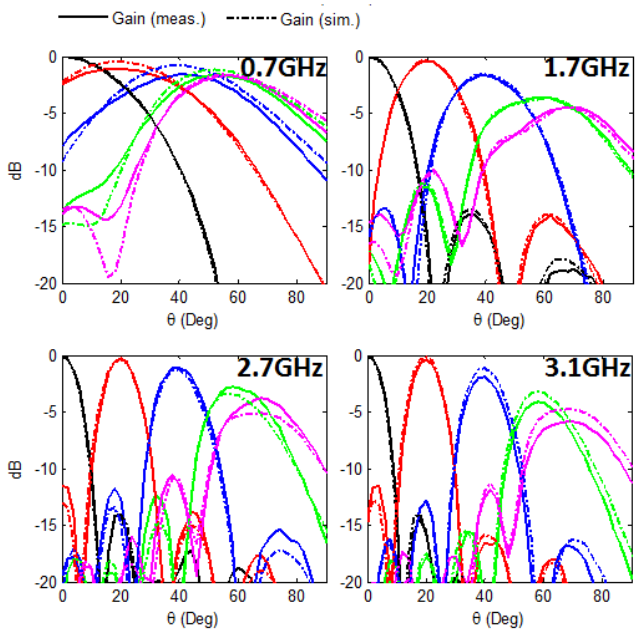

Fig. 14. Normalized patterns along the E plane for the active array. The array elements are phased for scan angles of 0°, 20°, 40°, 60°, and 70°.

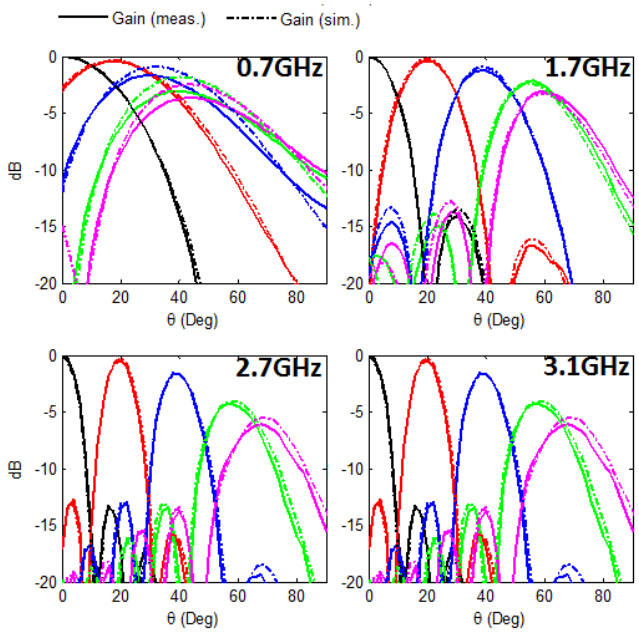

Fig. 15. Normalized patterns along the H plane for the active array. The array elements are phased for scan angles of 0°, 20°, 40°, 60°, and 70°.

when the array aperture is electrically small, the antenna can only scan up to moderate angles. However, the prototype can scan up to 70° at higher frequencies. We observe that sidelobes are at −13 dB for angles close to broadside as expected for a uniformly excited aperture; but increases for larger angles. We also note that the main beam broadens more than expected in the E plane at 70°. We believe that these degradations are due to the SW being stronger at larger scan angles. These SWs are not the well-known dielectric-guided waves [13] and exist only in finite arrays, due to reflections from the aperture edges [29].

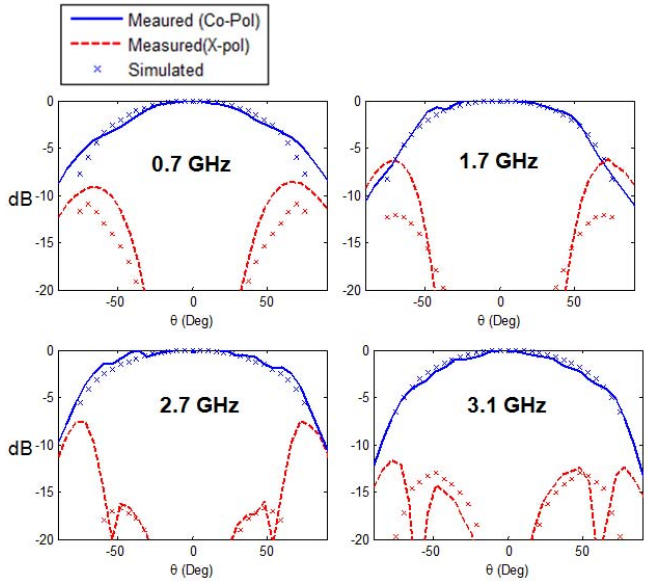

Fig. 16. D plane pattern for the central row along the diagonal of the aperture.

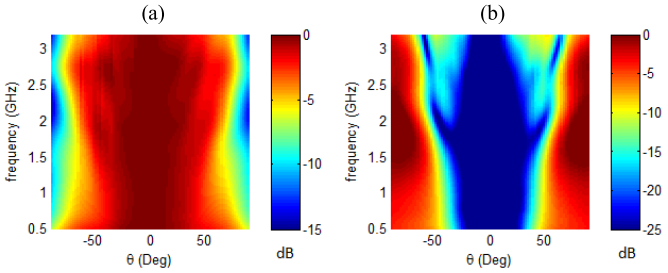

Fig. 17. D plane pattern across the whole scan volume and frequency range. (a) Normailzied co-pol. (b) Normalized X-pol.

It is possible to mitigate these waves by terminating a few elements from the edges with appropriate resistors as proposed in [29]. But since our prototype was already small at the lower end of the frequency band, we did not employ such edge termination.

As mentioned before, we only measured one row of elements along the aperture diagonal to obtain the D plane pattern. The measured 2-D patterns for the six-element row and simulated values for a single unit cell are depicted in Fig. 16. Excellent agreement is observed for co-pol gain values. However, the measured X-pol is higher predicted at the lower end of the band, for large elevation angles. We believe that this is due to the small ground plane. At higher frequencies, the measured X-pol levels align with the simulated values. The measured data across the entire frequency bandwidth and scan volume are provided in Fig. 17. We note that the normalized co-pol pattern indicates scanning capability up to 70° across most of the frequency range.

IV. Conclusion

A novel TCDA with integrated feed and FSS superstrate was presented. The feed structure was the widely used folded Marchand balun, but modified to facilitate wideband matching

at large scan angles. Infinite array simulations showed that the impedance bandwidth was more than 6:1 when scanning 75° in the E plane and 60° in the H plane. The FSS consisted of one conducting layer, which can be placed on the same PCB as the radiating elements and the feed lines. No dielectric slab was used for scan impedance compensation, implying a simple, lightweight, and low-cost array structure. We note that, additional circuitry for T/R modules or phase shifters can be placed on the same PCB extending below the ground plane, providing an extremely compact/integrated scanning array. Of course, this is true for relatively low frequencies (e.g., $f < 10$ GHz), where the vertical PCBs over metallic platforms can be practically implemented. For millimeter-wave applications, both the FSS layer and the feed-lines should be modified so that the overall array can be fabricated using multilayer planar/conformal PCBs.

A 12×12 prototype was designed, fabricated, and tested. The measured radiation patterns were compared to simulations. The 3 dB (compared to aperture directivity limit) gain bandwidth of the prototype was 6.9:1 for broadside radiation. Maximum scan angle was limited to about 50° due to electrically small size of the prototype at lower end of the frequency band. But ±70° scanning capability was verified at higher frequencies, for the two principal planes and the diagonal plane.

To our knowledge, the proposed TCDA is the first low-profile design to achieve more than 6:1 bandwidth with such wide scan angles (75° in E plane and 60° in H plane). This capability was achieved without using a bulky dielectric material over the aperture, making the proposed approach even more attractive.

REFERENCES

[1] G. C. Tavik *et al.*, "The advanced multifunction RF concept," *IEEE Trans. Microw. Theory Techn.*, vol. 53, no. 3, pp. 1009–1020, Mar. 2005.

[2] D. H. Schaubert, S. Kasturi, A. O. Boryssenko, and W. M. Elsallal, "Vivaldi antenna arrays for wide bandwidth and electronic scanning," in *Proc. 2nd Eur. Conf. Antennas Propag. (EuCAP)*, Nov. 2007, pp. 1–6.

[3] R. W. Kindt and W. R. Pickles, "Ultrawideband all-metal flared-notch array radiator," *IEEE Trans. Antennas Propag.*, vol. 58, no. 11, pp. 3568–3575, Nov. 2010.

[4] H. Holter, "Dual-polarized broadband array antenna with BOR-elements, mechanical design and measurements," *IEEE Trans. Antennas Propag.*, vol. 55, no. 2, pp. 305–312, Feb. 2007.

[5] R. Kindt and D. Taylor, "Polarization correction in dual-polarized phased arrays of flared notches," in *Proc. IEEE Int. Symp. Antennas Propag. Soc.*, Jul. 2011, pp. 1961–1964.

[6] M. W. Elsallal and J. C. Mather, "An ultra-thin, decade (10:1) bandwidth, modular 'BAVA' array with low cross-polarization," in *Proc. IEEE Antennas Propag. Soc. Int. Symp.*, Jul. 2011, pp. 1980–1983.

[7] A. Neto and J. J. Lee, "Ultrawide-band properties of long slot arrays," *IEEE Trans. Antennas Propag.*, vol. 54, no. 2, pp. 534–543, Feb. 2006.

[8] J. J. Lee, S. Livingston, and D. Nagata, "A low profile 10:1 (200–2000 MHz) wide band long slot array," in *Proc. IEEE Antennas Propag. Soc. Int. Symp.*, Jul. 2008, pp. 1–4.

[9] B. Munk *et al.*, "A low-profile broadband phased array antenna," in *Proc. IEEE Antennas Propag. Soc. Int. Symp.*, vol. 2. Jun. 2003, pp. 448–451.

[10] H. A. Wheeler, "Simple relations derived from a phased-array antenna made of an infinite current sheet," *IEEE Trans. Antennas Propag.*, vol. 13, no. 4, pp. 506–514, Jul. 1965.

[11] J. P. Doane, "Wideband low-profile antenna arrays: Fundamental limits and practical implementations," Ph.D. dissertation, Dept. Elect. Comput. Engrg., Ohio State Univ., Columbus, OH, USA, 2013.

[12] S. S. Holland and M. N. Vouvakis, "The planar ultrawideband modular antenna (PUMA) array," *IEEE Trans. Antennas Propag.*, vol. 60, no. 1, pp. 130–140, Jan. 2012.

[13] D. M. Pozar and D. H. Schaubert, "Scan blindness in infinite phased arrays of printed dipoles," *IEEE Trans. Antennas Propag.*, vol. 32, no. 6, pp. 602–610, Jun. 1984.

[14] J. P. Doane, K. Sertel, and J. L. Volakis, "A wideband, wide scanning tightly coupled dipole array with integrated balun (TCDA-IB)," *IEEE Trans. Antennas Propag.*, vol. 61, no. 9, pp. 4538–4548, Sep. 2013.

[15] N. Marchand, "Transmission-line conversion transformers," *Electronics*, vol. 17, pp. 142–145, Dec. 1944.

[16] D. Cavallo, A. Neto, and G. Gerini, "PCB slot based transformers to avoid common-mode resonances in connected arrays of dipoles," *IEEE Trans. Antennas Propag.*, vol. 58, no. 8, pp. 2767–2771, Aug. 2010.

[17] W. F. Moulder, K. Sertel, and J. L. Volakis, "Ultrawideband superstrate-enhanced substrate-loaded array with integrated feed," *IEEE Trans. Antennas Propag.*, vol. 61, no. 11, pp. 5802–5807, Nov. 2013.

[18] S. S. Holland, "Low-profile, modular, ultra-wideband phased arrays," Ph.D. dissertation, Dept. Math. Statistics, Univ. Massachusetts Amherst, Amherst, MA, USA, 2011.

[19] B. A. Munk, T. W. Kornbau, and R. D. Fulton, "Scan independent phased arrays," *Radio Sci.*, vol. 14, no. 6, pp. 979–990, Nov. 1978.

[20] S. D. Targonski, R. B. Waterhouse, and D. M. Pozar, "Design of wide-band aperture-stacked patch microstrip antennas," *IEEE Trans. Antennas Propag.*, vol. 46, no. 9, pp. 1245–1251, Sep. 1998.

[21] L. Infante, S. Mosca, and M. Teglia, "Low-profile wide-band wide-angle-scan antenna array element," in *Proc. 6th EUCAP*, Mar. 2012, pp. 638–642.

[22] D. Cavallo, W. H. Syed, H. T. Shivamurthy, and A. Neto, "A planar wideband wide-scan phased array: Connected array loaded with artificial dielectric layers," in *Proc. IEEE Int. Symp. Antennas Propag. Soc. (APSURSI)*, Jul. 2015, pp. 2523–2524.

[23] W. E. Kock, "Metallic delay lenses," *Bell Syst. Tech. J.*, vol. 27, no. 1, pp. 58–82, Jan. 1948.

[24] D. Cavallo, W. H. Syed, and A. Neto, "Closed-form analysis of artificial dielectric layers—Part II: Extension to multiple layers and arbitrary illumination," *IEEE Trans. Antennas Propag.*, vol. 62, no. 12, pp. 6265–6273, Dec. 2014.

[25] M. H. Novak and J. L. Volakis, "Ultrawideband antennas for multi-band satellite communications at UHF–Ku frequencies," *IEEE Trans. Antennas Propag.*, vol. 63, no. 4, pp. 1334–1341, Apr. 2015.

[26] J. A. Kasemodel, C.-C. Chen, and J. L. Volakis, "Wideband planar array with integrated feed and matching network for wide-angle scanning," *IEEE Trans. Antennas Propag.*, vol. 61, no. 9, pp. 4528–4537, Sep. 2011.

[27] A. Ludwig, "The definition of cross polarization," *IEEE Trans. Antennas Propag.*, vol. 21, no. 1, pp. 116–119, Jan. 1973.

[28] D. F. Kelley and W. L. Stutzman, "Array antenna pattern modeling methods that include mutual coupling effects," *IEEE Trans. Antennas Propag.*, vol. 41, no. 12, pp. 1625–1632, Dec. 1993.

[29] B. A. Munk, "Surface waves on passive surfaces of finite extent," in *Finite Antenna Arrays and FSS*, 1st ed. Hoboken, NJ, USA: Wiley, 2003, ch. 4, pp. 84–135.

Ersin Yetisir (S'11–M'16) received the B.Sc. degree in electrical and electronics engineering from Bilkent University, Ankara, Turkey, in 2010, and the Ph.D. degree from The Ohio State University, Columbus, OH, USA, in 2015.

He was a Graduate Research Assistant with the ElectroScience Laboratory, The Ohio State University, from 2010 to 2015, where he is currently a Post-Doctoral Researcher. His current research interests include wideband, low-profile antenna array and feed-network design for microwave and millimeter-wave frequencies, and wideband/multiband antennas with high isolation for MIMO and STAR applications.

Dr. Yetisir received best student paper awards from the 2016 USNC/URSI National Radio Science Meeting (second place) and the 2016 International Workshop on Antenna Technologies (co-author).

Nima Ghalichechian (S'99–M'08–SM'14) received the Ph.D. degree in electrical engineering from the University of Maryland, College Park, MD, USA, in 2007. His Ph.D. dissertation was titled "Design, Fabrication, and Characterization of a Rotary Variable-Capacitance Micromotor Supported on Microball Bearings."

He was with the Research Department, FormFactor Inc., Livermore, CA, USA, as a Senior Principal Engineer from 2007 to 2012. During this period, he helped design and develop microsprings for advanced probe cards used in testing memory and system-on-chip semiconductor devices. He joined The Ohio State University (OSU), ElectroScience Laboratory, Columbus, OH, USA, as a Research Scientist in 2012, where he is currently a Research Assistant Professor with the Department of Electrical and Computer Engineering. His research is interdisciplinary and centers around two areas of micro/nanotechnology and electromagnetics. Specifically, he conducts research on RF microsystems with focus on reconfigurable antenna arrays, millimeter-wave antennas, terahertz microsystems, sensors, novel materials, and microfabrication processes. As a Principal Investigator, he has led or helped establish several new programs with OSU sponsored by NSF, DARPA, and AFRL.

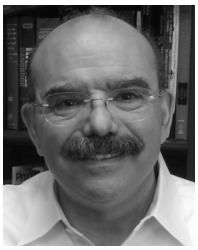

John L. Volakis (S'77–M'82–SM'89–F'96) was born in Chios, Greece, in 1956. He received the B.E. (*summa cum laude*) degree from Youngstown State University, Youngstown, OH, USA, in 1978, and the M.Sc. and Ph.D. degrees from The Ohio State University, Columbus, OH, USA, in 1979 and 1982, respectively.

He was with Boeing, Chicago, IL, USA, from 1982 to 1984. In 1984, he was appointed as an Assistant Professor with the University of Michigan, Ann Arbor, MI, USA, where he became a Full Professor in 1994. He served as the Director of the Radiation Laboratory from 1998 to 2000. Since 2003, he has been the Roy and Lois Chope Chair Professor of Engineering with The Ohio State University, where he currently serves as the Director of the ElectroScience Laboratory. Over the years, he carried out research in antennas, wireless communications and propagation, computational methods, electromagnetic compatibility and interference, design optimization, RF materials, multiphysics engineering, millimeter waves, terahertz, and medical sensing. He has authored eight books, 375 journal papers, nearly 700 conference papers, 26 book chapters, and 16 patents/patent disclosures. He has co-authored the books entitled *Approximate Boundary Conditions in Electromagnetics* (1995), *Finite Element Methods for Electromagnetics* (1998), *Antenna Engineering Handbook—Fourth Edition* (2007), *Small Antennas* (2010), and *Integral Equation Methods for Electromagnetics* (2011). He has graduated/mentored over 80 Ph.D. students/post-doctoral students with 34 of them receiving best paper awards at conferences.

Prof. Volakis is a Fellow of the Applied Computational Electromagnetics Society (ACES). He received the University of Michigan College of Engineering Research Excellence Award in 1993, the Scott Award from The Ohio State University College of Engineering for Outstanding Academic Achievement in 2011, the IEEE AP Society C-T. Tai Teaching Excellence Award in 2011, the IEEE Henning Mentoring Award in 2013, the IEEE Antennas and Propagation Distinguished Achievement Award in 2014, and the Ohio State University Distinguished Scholar Award in 2016. His service to professional societies includes serving as the President of the IEEE Antennas and Propagation Society (APS) in 2004, the Chair of the USNC/URSI Commission B from 2015 to 2017, twice the General Chair of the IEEE Antennas and Propagation Symposium, the IEEE APS Distinguished Lecturer, the IEEE APS Fellows Committee Chair, the IEEE-Wide Fellows Committee Member, and an Associate Editor of several journals. He was listed by ISI among the top 250 most referenced authors in 2004.